THE JOURNAL OF PHYSICAL CHEMISTRY B

Article

pubs.acs.org/JPCB

Role of Electronic-Vibrational Mixing in Enhancing Vibrational Coherences in the Ground Electronic States of Photosynthetic Bacterial Reaction Center

Ian Seungwan Ryu, Hui Dong, and Graham R. Fleming*

Department of Chemistry, University of California—Berkeley, and Physical Bioscience Division, Lawrence Berkeley National Laboratory, Berkeley, California 94720, United States

ABSTRACT: We describe polarization controlled two-color coherence photon echo studies of the reaction center complex from a purple bacterium *Rhodobacter sphaeroides*. Long-lived oscillatory signals that persist up to 2 ps are observed in neutral, oxidized, and mutant (lacking the special pair) reaction centers, for both (0°,0°,0°,0°) and (45°,−45°,90°,0°) polarization sequences. We show that the long-lived signals arise via vibronic coupling of the bacteriopheophytin (H) and accessory bacteriochlorophyll (B) pigments that leads to vibrational wavepackets in the B ground electronic state. Fourier analysis of the data suggests that the 685 cm^{-1} mode of B may play a key role in the H to B energy transfer.

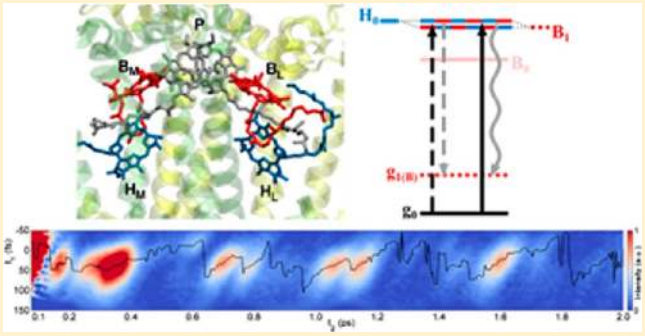

INTRODUCTION

Photosynthesis is a fundamental solar to chemical energy conversion process mediated by a sophisticated pigment−protein complex network. Photoexcitation of pigment molecules creates excitons which migrate toward a reaction center complex, where light-induced charge separation transforms light energy into chemical energy with near unity quantum efficiency.

The optical properties of pigment−protein complexes (PPCs) are governed by the excitonic structure determined from electronic couplings between densely packed pigment molecules. These couplings lead to delocalization of excited states (excitons), and excitation energy transfer (EET) rates are further optimized by the interplay between electronic couplings and pigment−protein interactions. Recent two-dimensional electronic spectroscopy (2DES) studies on various PPCs have revealed oscillating features in the two-dimensional (2D) spectra,[1−3] and a nondegenerate photon echo experiment showed coherence specific signals in the purple bacterial reaction center (bRC).[4] These experimental observations have been interpreted as a signature of electronic coherence, the coherent superposition between delocalized excited states (excitonic states).[5,6] Such excitonic coherences could allow electronic excitations move through PPCs like wavepackets maintaining their phase coherence. This quantum mechanically coherent nature of EET has been of great interest due to its potential contribution to the efficiency of photosynthetic EET.

One intriguing aspect of the experimentally observed signatures of coherence is their long lifetimes. The oscillations in 2D spectra of the Fenna−Matthews−Olson (FMO) complex lasted up to 1.2 ps (at 77 K),[7] and oscillations lasting over 1 ps (at 77 K) were observed in a 2DES study of the bacterial reaction center (bRC).[8] Such lifetimes are unexpectedly long for electronic coherences, longer than the presence of excited states in some cases, leading to the suggestion that some or perhaps all of the observed beats are of vibrational or vibronic origin.[9−16] In our view, despite significant contributions,[12,17−19] there is not yet a complete description of the interaction of high frequency (underdamped) nuclear motion and electronic mixing in donor−acceptor systems that fully incorporates the role of fluctuations on the vibronic coupling. Although vibrational wavepackets persist for several picoseconds in pigment−protein systems,[20−22] the influence of fluctuations on the resonance effects involved in mixing acceptor and donor modes is incompletely characterized. In a recent study, Dijkstra et al. showed that a critically underdamped nuclear mode can enhance energy transfer.[19] For example, two mechanisms for the enhancement of population transfer efficiency are identified: one when the frequency of the vibration matches the electronic energy gap, as expected, and one when the vibrational frequency satisfies the critical damping condition.

Similarly, the ability to distinguish electronic and nuclear wavepacket motion in experiment is not fully developed. Polarization controlled 2DES can distinguish pathways involving pure electronic coherences.[23,24] Once high frequency nuclear motions are introduced, however, the discrimination may be less than perfect. A second experimental approach is to use two nonoverlapping spectra to interrogate only coherence-related pathways.[4]

Received: October 9, 2013
Revised: January 16, 2014
Published: January 16, 2014

dx.doi.org/10.1021/jp4100476 | *J. Phys. Chem. B* 2014, 118, 1381−1388

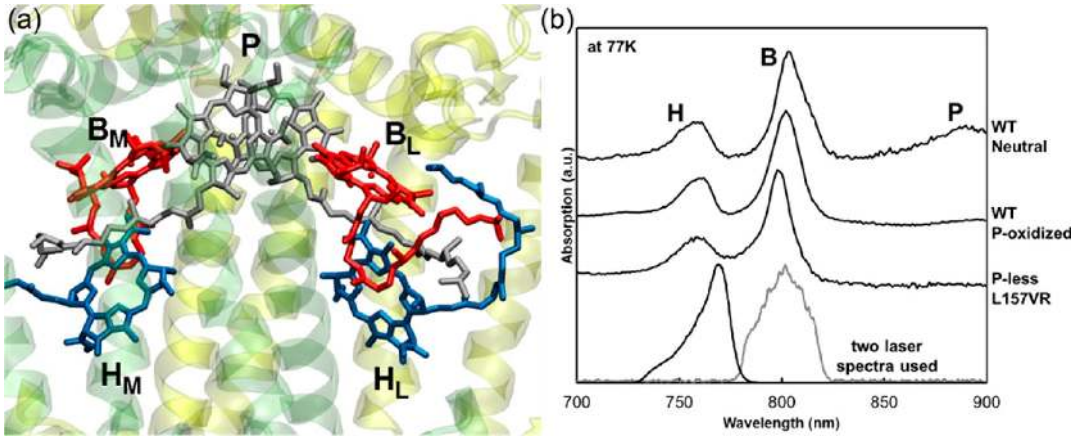

Figure 1. (a) The arrangement of chromophores responsible for Q_Y region absorption in bRC protein from *Rhodobacter sphaeroides* (PDB ID: 1PCR[28]). The subscripts L and M refer to the two branches of the symmetric arrangement of chromophores. Two BChls labeled as P are called the special pair, and serve a dual function as an excitonic energy acceptor and as the primary electron donor. (b) The absorption spectra of three bRC complex samples and the spectral profiles of the laser pulses used in the experiments. The B and H bands correspond to the excitations mainly on the accessory BChls (B_L and B_M) and the BPhys (H_L and H_M) molecules, respectively. The P band is only observed in the WT neutral bRC complex.

In this study, we use the two-color coherence photon echo method with the addition, as compared to previous work, of polarization control of the four light pulses involved. The combination of two-color excitation and polarization control enables the two-color coherence photon echo method to further isolate electronic and vibrational contributions. The polarization sequence(45°,−45°,90°,0°) discriminates in favor of coherences arising from pathways involving transition dipole moments that are not parallel to each other. In view of the well characterized ground state vibrational spectra of the chromophores and the previous two-color coherence photon echo study, we have applied this approach to the bRC complex from purple photosynthetic bacterium *Rhodobacter sphaeroides*.

To understand the observed signal from our experiments, it is important to note that the experimental design of the two-color coherence photon echo spectroscopy limits the possible coherences that can be prepared and contribute to the signal. In conventional 2DES, four degenerate laser pulses are used to interact with the entire excitonic manifold. Therefore, sequential light-matter interactions of the first and second laser pulses can create both population and coherence states within the excitonic state space. This approach can measure and provide a map of the entire excitonic dynamics because a broad laser spectrum induces all possible resonant interaction sequences. In two-color coherence photon echo spectroscopy of the bRC complex, the second laser pulse spectrum is not resonant with any states excited by the first laser pulse, preventing preparation of a population state. The same principle applies to the third and fourth interactions so that the detected coherent emission is not induced from a population state. Thus direct visualization of coherence dynamics is achieved with the two-color coherence photon echo technique.

EXPERIMENTAL SECTION

The chromophore assembly in the bRC protein complex from *Rhodobacter sphaeroides* is shown in Figure 1 with the absorption spectra of the three samples we studied. The six pigment molecules give rise to three well separated Q_Y absorption bands, which are labeled by the chromophore making the dominant contribution. The EET among them occurs sequentially from H to B (∼100 fs) and B to P (∼200 fs),[25] followed by charge separation from P. The charge separation occurs only along the L branch, and produces changes in the H and B band regions due to the B_L^- and H_L^- anion species formation, complicating the interpretation of spectral responses. Such a complication can be avoided by blocking the charge separation by chemically oxidizing P with potassium ferricyanide. Since P and P^+ are equally good excitonic energy quenchers, the oxidation of P to P^+ cation does not affect the EET dynamics.[26,27]

The EET dynamics in the bRC complex can also be modified by a mutagenesis approach. A mutant bRC strain L157VR, which lacks the two bacteriochlorophylls (BChls) composing P, exhibits dramatically increased excited state lifetimes for B. Replacing the valine residue at the L157 location by arginine places the arginine in the binding pocket for the P dimer, and only four pigments (two accessory BChls and two bacteriopheophytins (BPhys)) are present in the mutant L157VR bRC complex. The absence of the energy trap (P or P^+) leads to a lifetime of nearly 1 ns for the B band, while H to B energy transfer is not substantially altered.[26]

In this work, "neutral WT" represents the intact wild type (WT) bRC complex with the charge separation reaction present, and "P-oxidized WT" refers the wild type bRC complex whose charge separation is blocked. The P-less mutant bRC complex is labeled as "P-less L157VR".

The His-tagged bRC complex from *Rhodobacter sphaeroides* was prepared based on a previous description.[29] Cells cultured in the dark and a semiaerobic condition were harvested and homogenized, and the bRC proteins were solubilized by the lauryldimethylamine oxide (LDAO) and purified with a Ni-NTA column followed by FPLC. The samples were prepared in a glycerol/buffer (10 mM Tris HCl at pH 8.0 with 0.5% LDAO) (60/40, v/v) mixture placed between quartz windows, and cooled to 77 K using a cryostat (Oxford Instruments). The optical density at 800 nm was 0.2−0.3 at 77 K with a 0.2 mm path length. Sodium dithionite ($Na_2S_2O_4$) was added to a concentration of 5 mM for WT neutral bRC experiment to avoid the accumulation of P^+ cation.[30] For P-oxidized WT bRC experiment, $K_3Fe(CN)_6$ was added to ∼300 mM to chemically oxidize P.

dx.doi.org/10.1021/jp4100476 | J. Phys. Chem. B 2014, 118, 1381−1388

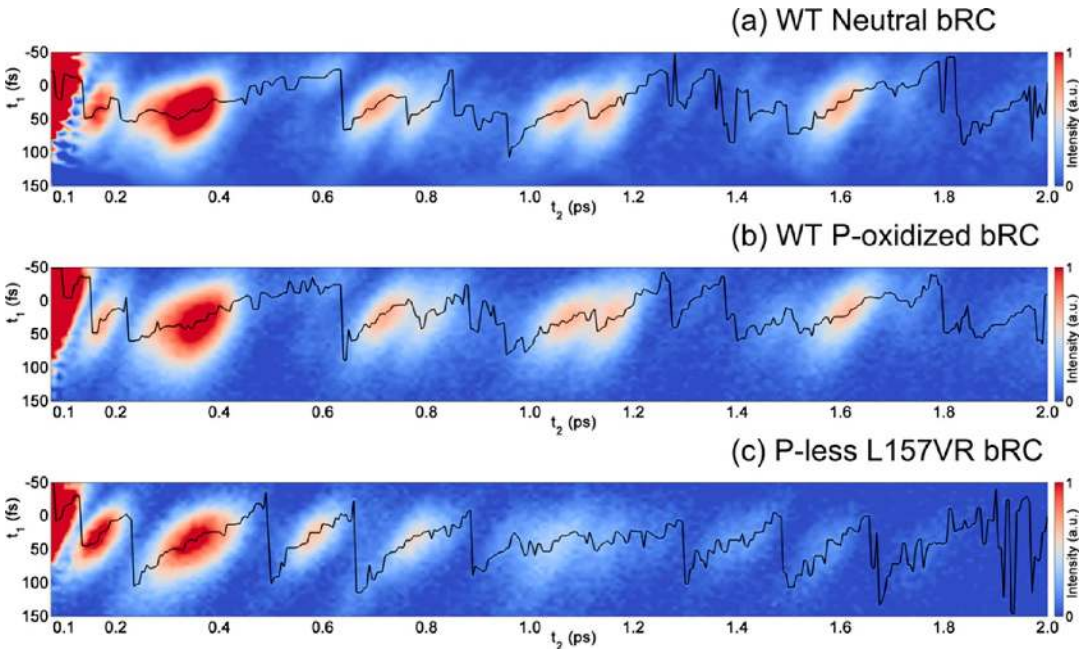

Figure 2. The two-color coherence photon echo integrated signals as a function of the two time delays t_1 and t_2, from (a) WT neutral bRC, (b) WT P-oxidized bRC, and (c) P-less L157VR mutant bRC complexes. The black lines follow the maximum of the echo signal at a given t_2. The pulse ordering for all experiments was 770 (k_1) − 800 (k_2) − 770 (k_3) − 800 (k_s) (in nm), and all the polarizations were set to be parallel to each other, i.e. (0°,0°,0°,0°). The t_2 axis represents the evolution of the initially prepared coherence. The data for t_2 < 100 fs are not shown (see text).

A commercial regenerative amplifier (Coherent) running at 1 kHz provided 800 nm pulses and pumped an optical parametric amplifier (Coherent) to generate 770 nm pulses. Both 800 and 770 nm were compressed to ∼45 fs by independent prism compression lines. Optical filters with a 25 nm fwhm bandwidth were used to prevent spectral overlap between the pulses of the two different center wavelengths (see Figure 1(b)). Three pulses, arranged in equilateral triangle geometry, were focused onto the sample with pulse energy of 5 nJ for each. The time-integrated photon echo signals, as a function of t_1 and t_2, were collected with a photomultiplier tube (Hamamatsu) using lock-in amplification with an optical chopper. An optical bandpass filter centered at 800 nm with 25 nm fwhm bandwidth was placed in front of the photomultiplier tube to detect signals from the coherence pathways only. For the polarization controlled experiments, a linear polarizer was placed along each laser beam traveling path. An additional fourth linear polarizer was placed in front of the photomultiplier tube as an analyzer. The contrast ratio of each polarizer was found to be at least 1000:1 within an error of ±1°. The >1 ps signal intensity is >25% which is substantially higher than the potentially leaked signal amplitude from imperfect polarizer excitation.

RESULTS AND DISCUSSION

In this study, the first pulse (k_1) was tuned to be centered at 770 nm (black line in Figure 1 (b)), which is resonant to the H transition, and the second pulse (k_2) is tuned to the B transition at 800 nm (gray line in Figure 1 (b)). The third pulse (k_3) arrives at the sample after a delay time (t_2) to probe changes in the initially prepared coherence states. The first and third pulses are spectrally identical (770 nm) and the generated photon echo signal field passes a bandpass filter centered at 800 nm. Population related pathways, such as electronic population relaxation from H to B, do not contribute to the detected signal due to the phase matching condition and the pulse ordering.

Figure 2 shows the coherence photon echo signal intensity map from the three bRC complexes as a function of two time delays (t_1 and t_2). The most prominent feature is the existences of a periodic signal up to nearly $t_2 \approx 2$ ps in all three bRC complexes. When electronic transitions are considered alone, only the $|B\rangle\langle H|$ coherence is optically accessible via the first (H transition) and second (B transition) interactions. However, the $|B\rangle\langle H|$ coherence cannot be the origin of the signal at t_2 times exceeding the lifetimes of the B and H excitonic states.

We can make a simple estimate of the maximum duration of a pure electronic coherence as follows. The population relaxation times of the B and H excitonic states have been measured to be 150 and 100 fs, respectively.[25−27] The simplest description of the $|B\rangle\langle H|$ coherence decay time (τ_{BH}) is given by the following:

$$\frac{1}{\tau_{BH}} = \frac{1}{2}\left(\frac{1}{\tau_B} + \frac{1}{\tau_H}\right) + \frac{1}{\tau_{decoherence}} \quad (1)$$

where τ_B and τ_H refer population relaxation times of B and H excitonic states respectively, and $1/\tau_{decoherence}$ denotes the pure decoherence rate.[31] Even though the pure decoherence rate is not known, the upper limit for the $|B\rangle\langle H|$ coherence lifetime can be estimated by assuming the pure decoherence rate to be zero ($\tau_{decoherence} \approx \infty$). Then the longest possible lifetime for the $|B\rangle\langle H|$ coherence is <150 fs, almost an order of magnitude shorter than the observed signal lifetimes of near 2 ps.

Additionally, no change in the coherence photon echo signal was observed whether the special pair BChl dimer (P) was chemically oxidized or not. This is consistent with a ground state vibrational origin for the long-lived features in Figure 2. The data from the P-less L157VR (Figure 2 (c)) further support this conclusion. Despite the increase in the excited state lifetime of B by more than 3 orders of magnitude, the

dx.doi.org/10.1021/jp4100476 | J. Phys. Chem. B 2014, 118, 1381−1388

coherence signal also lasted for 2 ps, similar to the WT bRC complexes. We note, to avoid potential confusion, that these conclusions are not intended to apply to the short time region (t_2 < 150 fs) of the data. Due to the spectral requirement of the method, the short time region free from pulse overlap effects is not accessible. In the pulse overlap region, the photon echo signal related to the population pathway overwhelms the coherence signal due to the imperfect pulse orderings.

Vibrational wavepackets can be created either in the excited or ground electronic states but, of course, the lifetimes of vibrational coherences in an excited state are also limited by the excited state population relaxation time,[32] which is less than 200 fs in WT bRC complexes as noted above. Therefore, we conclude that the long-term oscillatory signals from the bRC complexes mainly reflect vibrational wavepackets in the ground electronic state of the accessory bacteriochlorophyll.

ELECTRONIC-VIBRATIONAL MIXING

Consider the simplified level scheme shown in Figure 3(a). Here, $|g_0\rangle$ is the ground electronic state, $|H_0\rangle$ is the vibrationally unexcited, electronically excited state of H, and $|B_1\rangle$ is a vibrational level of excited B roughly resonant with $|H_0\rangle$ and $|g_{1(B)}\rangle$ is a ground electronic state vibrational level of B. The Feynman diagram in Figure 3(b) shows a rephasing pulse sequence that leads to a $|g_0\rangle\langle g_{1(B)}|$ ground state coherence through the electronic-vibrational mixing of $|H_0\rangle$ and $|B_1\rangle$ Clearly, the magnitude of the contribution of ground state vibrational wavepackets will depend on the strength of the electronic coupling, the deviation from resonance, and the influence of fluctuations. The electronic coupling between H and B is estimated to be 200−250 cm^{-1},[33,34] allowing reasonable coupling between vibrationally unexcited, electronically excited H and v = 1 or v = 2 of excited B even for the very small Franck−Condon factors associated with these transitions from the B ground state. In fact, the very small Franck−Condon factor for $\langle n|m\rangle$ ($n \neq m$) makes the preparation of the ground state vibrational coherence more likely as the Franck−Condon factor is larger for a $\langle n|n\rangle$ transition than $\langle n|m\rangle$ transition.

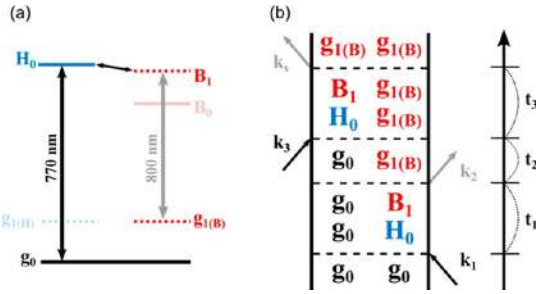

Figure 3. (a) Simplified energy level scheme to illustrate electronic-vibrational mixing: the double headed arrow connecting the H_0 and B_1 states. (b) A double sided Feynman diagram describing the Liouville pathway for the creation of a vibrational wavepacket on the B ground electronic state during t_2.

Vibrational wavepackets in molecular ground electronic states are commonly observed via impulsive stimulated Raman scattering (ISRS),[15] which does not require electronic-vibrational mixing. If the transition dipole moments of the acceptor vibration are unperturbed, then we can consider only electronic transitions in calculating the influence of specific polarization sequences. In this case, the dependence of Liouville pathways on the linear polarizations of laser pulses and relative orientations of transition dipole moments is described by their polarization prefactor, determined by eq 2.[23]

$$\langle \mathbf{abcd} \rangle \equiv \langle (\hat{\mu}_\mathbf{a} \times \hat{E}_1)(\hat{\mu}_\mathbf{b} \times \hat{E}_2)(\hat{\mu}_\mathbf{c} \times \hat{E}_3)(\hat{\mu}_\mathbf{d} \times \hat{E}_4) \rangle \qquad (2)$$

In this equation, $\hat{\mu}_i$ refers the unit vector for the transition dipole moment of i transition, and $\hat{E}_n$ refers the linear polarization direction of the n-th laser pulse. We consider four pathways in Figure 4. These involve electronic coherence between B and H (R_1), an excited state vibrational wavepacket in B (R_2), ISRS on H to create a ground vibrational wavepacket on H (R_3), and electronic mixing between H and B leading to a ground electronic state B vibrational wavepacket (R_4). The calculated polarization prefactors for these four pathways are shown in Table 1. Under the so-called "coherence specific"

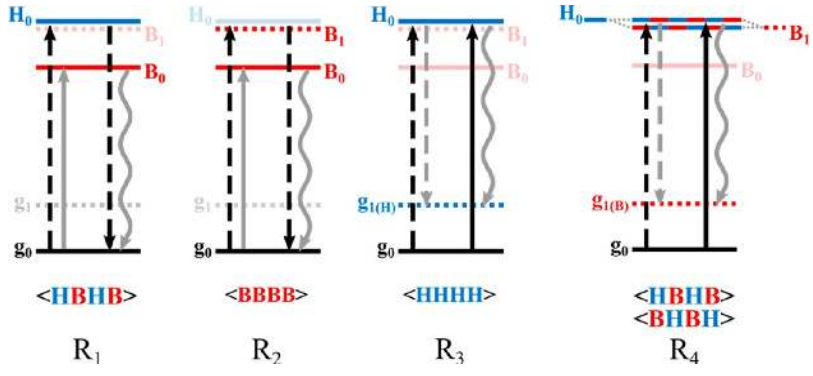

Figure 4. Possible Liouville pathways for the two-color coherence photon echo spectroscopy. The model assumes excitonic dimer (B and H) and includes a discrete vibrational mode. The frequency of the vibration was chosen to be similar to the excitonic energy gap between B and H. The arrows in diagrams refer the laser pulse and echo signal fields (black: 770 nm, gray: 800 nm), and arranged according to the pulse ordering used in the experiments (k_1~k_4 from left to right). The energy levels that are not directly associated to the process is in faint colors. The transition dipole moment prefactor for each pathway is written under the diagram. B and H transition dipole moments are denoted by red and blue, respectively. Each pathway represents different types of coherences that can be excited in the two-color coherence photon echo. R_1: electronic coherence, R_2: vibrational coherence in the excited state, R_3: vibrational coherence in the ground electronic state (by ISRS), R_4: vibrational coherence in the ground electronic state (by electronic-vibrational mixing). For R_4, two alternating colors are used to indicate the electronic-vibrational mixing, and the ladder diagram is equivalent to the double sided Feynman diagram shown in Figure 3(b).

dx.doi.org/10.1021/jp4100476 | J. Phys. Chem. B 2014, 118, 1381−1388

Table 1. Calculated Polarization Prefactors for the Polarization Sequences Used in the Experiments[a]

	Polarization Configuration				Transition Dipole Moment Orientational Factors		
	k_1	k_2	k_3	k_s	<HHHH> <BBBB>	<HHBB> <BBHH>	<HBHB> <BHBH>
<1>	0°	0°	0°	0°	1/5	1/15	1/15
<2>	45°	-45°	90°	0°	0	0	1/12
	Relevant Pathways:				R_2, R_3	population pathways	R_1, R_4

[a]It was assumed that the two transition dipole moments of B and H excitations are orthogonal, and vibrationally excited transitions have similar spatially orientations to the purely electronic transitions.

polarization configuration,[24,35] $(\hat{E}_1, \hat{E}_2, \hat{E}_3, \hat{E}_4)$ = (45°,−45°,90°,0°), all of the orientationally averaged prefactors become zero, except the pathways for electronic coherence (R_1 in Figure 4), and vibrational coherence in the electronic ground state enhanced by electronic-vibrational mixing (R_4). Thus, suppression of the signal intensity is expected under the (45°,−45°,90°,0°) polarization configuration if the observed coherence in Figure 2 is related to ISRS (R_3) or vibrational coherence in the excited state (R_2) pathways.

The coherence photon echo spectra for the bRC complexes taken with the (45°,−45°,90°,0°) polarization configuration are shown in Figure 5(a),(c). Compared to the all parallel polarization (0°,0°,0°,0°) data shown in Figure 2, the changes in the coherence signals are small. The signal amplitudes for the (0°,0°,0°,0°) and (45°,−45°,90°,0°) polarizations are compared in Figure 5(b),(e). To facilitate the comparison, the echo signal was integrated over t_1 at a given t_2, better reflecting the overall signal intensity change along t_2. Notable differences seen in Figure 5(b) between the two polarization sequences are the decreased amplitude of the first peak at $t_2 \approx 200$ fs and the absence of the peak with small amplitude at $t_2 \approx 600$ fs under the (45°,−45°,90°,0°) polarization. Similar changes are observed in the data from the P-less L157VR mutant (Figure 5 (e)). The small changes observed in the coherence echo data under the (45°,−45°,90°,0°) polarization configuration suggest that the majority of the detected coherence signal requires two nonparallel transition dipole moments, strongly indicating the presence of the electronic-vibrational mixing mechanism. Additionally, the similarities between the data from (45°,−45°,90°,0°) and (0°,0°,0°,0°) polarizations are further explained by considering the contribution from Franck−Condon integrals of pathways described in Figure 4. The value of a Franck−Condon overlap integral for a transition between two electronic states depends on the zero-point displacement.[36,37] For a system with small zero-point displacements (small Huang−Rhys factors), such as B and H transitions of the bRC complex,[38] the Franck−Condon contributions in R_2 and R_3 pathways are much smaller than R_1 and R_4 pathways. As a result, we expect the R_1 and R_4 pathways to make the dominant contribution to the echo signal amplitude even in the (0°,0°,0°,0°) polarization condition.

We note that the amplitudes of the peak at t_2 = 600 fs provides information on vibrational coherence in the B excited electronic state. Under the (45°,−45°,90°,0°) polarization condition, the peak at t_2 = 600 fs is absent in the data from both WT bRC and P-less L157VR mutant complexes (Figure 5(b),(e) blue lines). However, it has larger amplitude in the

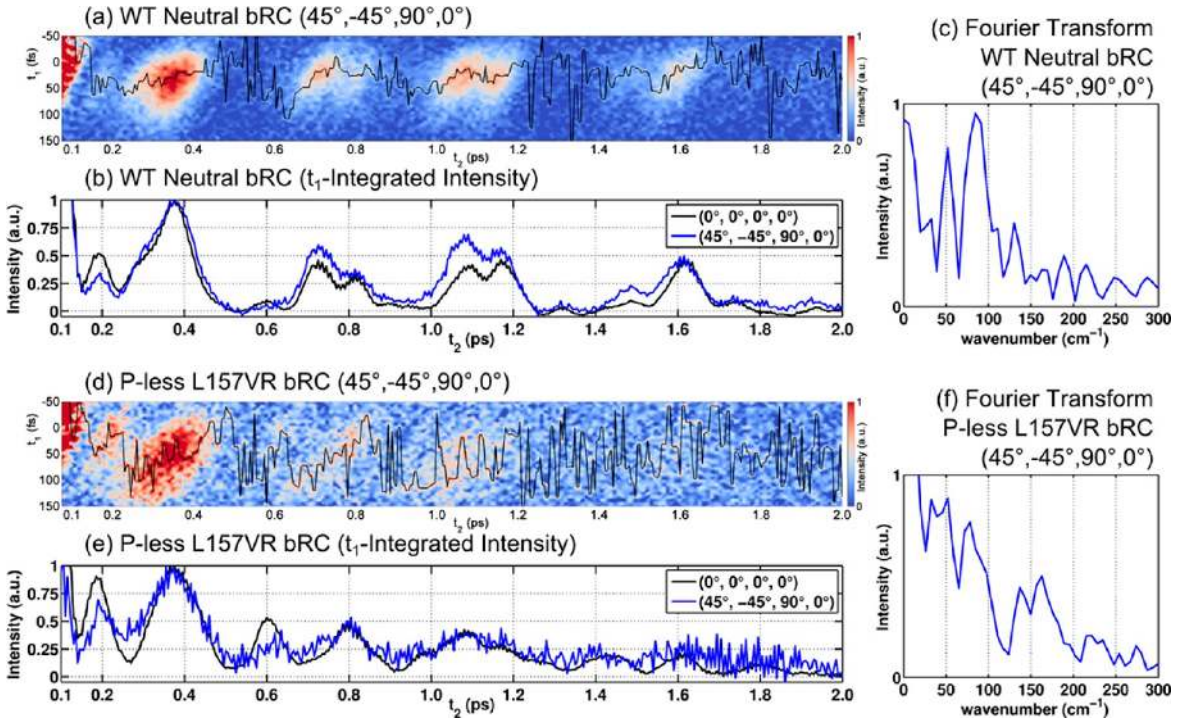

Figure 5. Two-color coherence photon echo integrated signals under the (45°,−45°,90°,0°) polarization configuration as a function of time delays t_1 and t_2, from (a) WT neutral bRC (d) P-less L157VR mutant bRC complexes. WT P-oxidized bRC data is identical to the WT neutral bRC (data not shown). The black lines follow the maximum of the echo signal at a given t_2. The pulse ordering for all experiments was 770 (k_1) − 800 (k_2) − 770 (k_3) − 800 (k_s) (in nm). The t_1-integrated coherence echo signal intensities from (b) WT neutral bRC (e) P-less L157VR mutant bRC complexes shows differences between the (0°,0°,0°,0°) (black) and (45°,−45°,90°,0°) (blue) polarization configurations. The absolute signal amplitude is 3−4 times weaker under the (45°,−45°,90°,0°) polarization than the (0°,0°,0°,0°) polarization. The Fourier transform power spectra of the (45°,−45°,90°,0°) polarization data in (b) and (e) are shown in (c) and (f), respectively.

dx.doi.org/10.1021/jp4100476 | J. Phys. Chem. B 2014, 118, 1381−1388

data from P-less L157VR mutant than from the WT bRC complex (Figure 5(b),(e) black lines) under the all-parallel polarization (0°,0°,0°,0°). This can be understood as a vibrational coherence on the excited states (R_2 in Figure 4), whose intensity will be small in the WT bRC complexes due to the rapid loss of the B excited state population.

Figure 5 also shows the Fourier transform power spectra of the time-dependent data for the WT neutral bRC (e) and the P-less L157VR mutant (f).

■ ORIGIN OF THE OBSERVED FREQUENCIES

The two-color coherence photon echo measurement is a homodyne measurement in which the echo intensity is measured, rather than the signal field. This means that the characteristic oscillations of superposition states appear as $|e^{i\omega_1 t_2} + e^{i\omega_2 t_2} + e^{i\omega_3 t_2} + ...|^2 = 2\cos[(\omega_1 - \omega_2)t_2] + 2\cos[(\omega_1 - \omega_3)t_2] + ...$ As a result, differences between system's oscillation frequencies will be found in the homodyne signal intensity oscillations.

The full width at half maxima (fwhm) of the two laser spectra centered at 770 and 800 nm, respectively, provide the range of accessible energy gap values (300−850 cm^{-1}) for the two energy levels that can be coherently excited. Thus only vibrational modes with relatively high-frequencies ($\gg k_B T$) need to be considered. Also, the 770 nm laser pulse was chosen to excite the red-side of the H band, allowing us to focus on high-frequency vibrations activated via the B band excitation. Resonance Raman studies of the bRC complex have identified multiple vibrational frequencies associated to the B band, and the four strong modes in the accessible energy gap window (566, 685, 735, 764 cm^{-1}) can be considered as candidates for the observed vibrational coherence.[38,39] These four Raman mode frequencies are also in agreement with the oscillation frequencies found in the recent 2DES studies of the bRC complex.[8] The Fourier transforms of the coherence photon echo signal beating along t_2 (Figure 5(c),(f)) showed three frequency components of 50, 80, and 125 cm^{-1}. These three frequencies are in good agreement with the differences obtained from the strong Raman frequencies (685−566 = 119 cm^{-1} ; 735−685 = 50 cm^{-1}; 764−685 = 79 cm^{-1}).

Of the six frequency differences possible from four frequencies, only three are clearly identified in the Fourier transform. Notably, all three involve the 685 cm^{-1} mode, indicating that 685 cm^{-1} mode is the most strongly activated one. Then 685 cm^{-1} mode can be considered as the primary vibrational mode comprising the electronic-vibrational mixing. The mixing can be further assisted by the fact that 685 cm^{-1} is close to the B and H excitonic energy gap value of 665 cm^{-1}.

Previous studies on coherence dynamics in the bRC complex suggested picosecond-long electronic coherence lifetimes[8] and proposed correlated protein environment for coherence protection.[4] However, suggestions did not conclude the role of vibronic coupling on the energy transfer dynamics. In the contrast, we conclude that any $|B\rangle\langle H|$ electronic coherence contribution to the observed signal is limited to the very early t_2 time window, as expected from the population dynamics. Since the $|B\rangle\langle H|$ electronic coherence pathway (R_1) involves two strongly resonant transitions, the strength of the signal at short time (in the absence of decoherence) is expected to be larger than the electronic-vibrational mixing pathway (R_4). The electronic-vibrational mixing involving the 0−1 transition of the 685 cm^{-1} mode, for example, enhances the contribution of this mixing, which has less than 5% of the 0−0 transition probability without mixing.[40] Such a small transition probability will be enhanced by coupling to the neighboring strongly allowed $|g\rangle \rightarrow |H\rangle$ transition, but is expected to be smaller than the pathways fully composed of the stronger 0−0 electronic transitions. Clearly, quantitative calculations are required to confirm these qualitative statements.

The observed coherence photon echo signal clearly demonstrates that the bRC excitation dynamics involve the electronic-vibrational mixing. The role of such electronic-vibrational mixing for the EET dynamics in the bRC complex were explored in other studies, and the vibronic rate enhancement effect was suggested to explain the EET dynamics of a photosynthetic light harvesting complex with a relatively large excitonic energy gap.[41,42] Also several theoretical studies implied that the vibronic interaction could be potentially important in achieving ultrafast EET rates in the bRC complex.[33,43]

One natural question arising from this observation is how universal such an electronic-vibrational mixing mechanism is in photosynthetic PPCs. We note that the excitonic structure and function of the bRC complex is distinct from other light harvesting PPCs. The estimated electronic coupling constant between the accessory BChl and the BPhy ranges from 200 to 250 cm^{-1},[33,34] which is significantly larger than electronic coupling constants determined for the Fenna−Matthew−Olson complex and the light harvesting complex II.[44,45] The function of the bRC complex is to perform rapid and irreversible charge separation. This involves chemically different species as donors and acceptors, and corresponding large energy gaps. In light harvesting complexes, these are generally large assemblies of chemically identical species with energy gaps determined by the combination of site energies and electronic couplings. A strong role for high frequency, underdamped vibration seems less likely in this case. An exception might be, however, the energy transfer from chlorophyll a to chlorophyll b in the light harvesting complex II (LHC II) where the energy gap is about 600 cm^{-1}.[45]

■ CONCLUSIONS

We have demonstrated the presence of electronic-vibrational coupling between the bacteriopheophytin and the accessory bacteriochlorophyll in the bRC complex. The vibrational mode with a ground state frequency of 685 cm^{-1} from the accessory bacteriochlorophyll is observed (via different frequencies) prominently. Oscillations involving different frequencies with this mode do not appear strongly in one-color three photon echo peak shift measurement,[34] suggesting that the mixing with the bacteriopheophytin is responsible for its appearance in the two-color coherence photon echo experiments. Since the frequency of this mode is similar to the energy gap of H and B, the vibrational modes in ground electronic state can be activated via stimulated emission.[12,46] However, a full understanding of the interplay between electronic and vibrational excitations in energy transfer processes remains, in our opinion, to be developed. We believe the data presented here can be used to calibrate theoretical approaches and lead to a deeper understanding of photosynthetic light harvesting.

■ AUTHOR INFORMATION

Corresponding Author

*E-mail: GRFleming@lbl.gov.

Notes

The authors declare no competing financial interest.

■ ACKNOWLEDGMENTS

This work was supported by the Director, Office of Science, and Office of Basic Energy Sciences of the U.S. Department of Energy under Contract DE-AC02-05CH11231 and by the Division of Chemical Sciences, Geosciences, and Biosciences and Office of Basic Energy Sciences of the U.S. Department of Energy through Grant DE-AC03-76SF000098. We thank S.G. Boxer for *Rhodobacter sphaeroides* strains; and S. Marqusee and K. Hart for their help with sample preparations.

■ REFERENCES

(1) Engel, G. S.; Calhoun, T. R.; Read, E. L.; Ahn, T.-K.; Mancal, T.; Cheng, Y.-C.; Blankenship, R. E.; Fleming, G. R. Evidence for Wavelike Energy Transfer Through Quantum Coherence in Photosynthetic Systems. *Nature* **2007**, *446*, 782−786.

(2) Calhoun, T. R.; Ginsberg, N. S.; Schlau-Cohen, G. S.; Cheng, Y.-C.; Ballottari, M.; Bassi, R.; Fleming, G. R. Quantum Coherence Enabled Determination of the Energy Landscape in Light-Harvesting Complex II. *J. Phys. Chem. B* **2009**, *113*, 16291−16295.

(3) Collini, E.; Wong, C. Y.; Wilk, K. E.; Curmi, P. M. G.; Brumer, P.; Scholes, G. D. Coherently Wired Light-Harvesting in Photosynthetic Marine Algae at Ambient Temperature. *Nature* **2010**, *463*, 644−647.

(4) Lee, H.; Cheng, Y.-C.; Fleming, G. R. Coherence Dynamics in Photosynthesis: Protein Protection of Excitonic Coherence. *Science* **2007**, *316*, 1462−1465.

(5) Cheng, Y.-C.; Fleming, G. R. Dynamics of Light Harvesting in Photosynthesis. *Annu. Rev. Phys. Chem.* **2009**, *60*, 241−262.

(6) Ishizaki, A.; Fleming, G. R. Quantum Coherence in Photosynthetic Light Harvesting. *Annu. Rev. Cond. Mat. Phys.* **2012**, *3*, 333−361.

(7) Panitchayangkoon, G.; Hayes, D.; Fransted, K. A.; Caram, J. R.; Harel, E.; Wen, J.; Blankenship, R. E.; Engel, G. S. Long-Lived Quantum Coherence in Photosynthetic Complexes at Physiological Temperature. *Proc. Natl. Acad. Sci., U. S. A.* **2010**, *107*, 12766−12770.

(8) Westenhoff, S.; Paleček, D.; Edlund, P.; Smith, P.; Zigmantas, D. Coherent Picosecond Exciton Dynamics in a Photosynthetic Reaction Center. *J. Am. Chem. Soc.* **2012**, *134*, 16484−16487.

(9) Christensson, N.; Kauffmann, H. F.; Pullerits, T.; Mančal, T. Origin of Long-lived Coherences in Light-Harvesting Complexes. *J. Phys. Chem. B* **2012**, *116*, 7449−7454.

(10) Huo, P.; Coker, D. F. Influence of Environment Induced Correlated Fluctuations in Electronic Coupling on Coherent Excitation Energy Transfer Dynamics in Model Photosynthetic Systems. *J. Chem. Phys.* **2012**, *136*, 115102.

(11) Kim, H. W.; Kelly, A.; Park, J. W.; Rhee, Y. M. All-Atom Semiclassical Dynamics Study of Quantum Coherence in Photosynthetic Fenna−Matthews−Olson Complex. *J. Am. Chem. Soc.* **2012**, *134*, 11640−11651.

(12) Tiwari, V.; Peters, W. K.; Jonas, D. M. Electronic Resonance with Anticorrelated Pigment Vibrations Drives Photosynthetic Energy Transfer Outside the Adiabatic Framework. *Proc. Natl. Acad. Sci., U. S. A.* **2013**, *110*, 1203−1208.

(13) Chin, A. W.; Prior, J.; Rosenbach, R.; Caycedo-Soler, F.; Huelga, S. F.; Plenio, M. B. The Role of Non-Equilibrium Vibrational Structures in Electronic Coherence and Recoherence in Pigment−Protein Complexes. *Nat. Phys.* **2013**, *9*, 113−118.

(14) Chenu, A.; Christensson, N.; Kauffmann, H. F.; Mančal, T. Enhancement of Vibronic and Ground-state Vibrational Coherences in 2D Spectra of Photosynthetic Complexes. *Sci. Rep.* **2013**, *3*, 2029.

(15) Calhoun, T. R.; Davis, J. a.; Graham, M. W.; Fleming, G. R. The Separation of Overlapping Transitions in β-Carotene with Broadband 2D Electronic Spectroscopy. *Chem. Phys. Lett.* **2012**, *523*, 1−5.

(16) Richards, G. H.; Wilk, K. E.; Curmi, P. M. G.; Quiney, H. M.; Davis, J. A. Coherent Vibronic Coupling in Light-Harvesting Complexes from Photosynthetic Marine Algae. *J. Phys. Chem. Lett.* **2012**, *3*, 272−277.

(17) Jean, J. M.; Fleming, G. R. Competition Between Energy and Phase Relaxation in Electronic Curve Crossing Processes. *J. Chem. Phys.* **1995**, *103*, 2092.

(18) Biggs, J. D.; Cina, J. A. Studies of Impulsive Vibrational Influence on Ultrafast Electronic Excitation Transfer. *J. Phys. Chem. A* **2012**, *116*, 1683−1693.

(19) Dijkstra, A. G.; Cao, J.; Fleming, G. R. Exciton Dynamics in the Presence of Colored Noise from Underdamped Vibrations. 2013, arXiv:*1309*.4910 [physics.chem−ph].

(20) Vos, M. H.; Rappaport, F.; Lambry, J.-C.; Breton, J.; Martin, J.-L. Visualization of Coherent Nuclear Motion in a Membrane Protein by Femtosecond Spectroscopy. *Nature* **1993**, *363*, 320−325.

(21) Wang, Q.; Schoenlein, R.; Peteanu, L.; Mathies, R.; Shank, C. Vibrationally Coherent Photochemistry in the Femtosecond Primary Event of Vision. *Science* **1994**, *266*, 422−424.

(22) Zhu, L.; Sage, J.; Champion, P. Observation of Coherent Reaction Dynamics in Heme Proteins. *Science* **1994**, *266*, 629−632.

(23) Hochstrasser, R. M. Two-Dimensional IR-Spectroscopy: Polarization Anisotropy Effects. *Chem. Phys.* **2001**, *266*, 273−284.

(24) Schlau-Cohen, G. S.; Ishizaki, A.; Calhoun, T. R.; Ginsberg, N. S.; Ballottari, M.; Bassi, R.; Fleming, G. R. Elucidation of the Timescales and Origins of Quantum Electronic Coherence in LHC II. *Nat. Chem.* **2012**, *4*, 389−395.

(25) Vos, M. H.; Breton, J.; Martin, J. Electronic Energy Transfer within the Hexamer Cofactor System of Bacterial Reaction Centers. *J. Phys. Chem. B* **1997**, *101*, 9820−9832.

(26) Jackson, J. A.; Lin, S.; Taguchi, A. K. W.; Williams, J. C.; Allen, J. P.; Woodbury, N. W. Energy Transfer in *Rhodobacter sphaeroides* Reaction Centers with the Initial Electron Donor Oxidized or Missing. *J. Phys. Chem. B* **1997**, *101*, 5747−5754.

(27) Arnett, D. C.; Moser, C. C.; Dutton, P. L.; Scherer, N. F. The First Events in Photosynthesis: Electronic Coupling and Energy Transfer Dynamics in the Photosynthetic Reaction Center from *Rhodobacter sphaeroides*. *J. Phys. Chem. B* **1999**, *103*, 2014−2032.

(28) Ermler, U.; Fritzsch, G.; Buchanan, S. K.; Michel, H. Structure of the Photosynthetic Reaction Centre from *Rhodobacter sphaeroides* at 2.65 Å Resolution: Cofactors and Protein-Cofactor Interactions. *Structure* **1994**, *2*, 925−936.

(29) Goldsmith, J. O.; Boxer, S. G. Rapid Isolation of Bacterial Photosynthetic Reaction Centers with an Engineered Poly-Histidine Tag. *Biochim. Biophys. Acta* **1996**, *1276*, 171−175.

(30) King, B. A.; McAnaney, T. B.; de Winter, A.; Boxer, S. G. Excited-State Energy Transfer Pathways in Photosynthetic Reaction Centers: 5. Oxidized and Triplet Excited Special Pairs as Energy Acceptors. *Chem. Phys.* **2003**, *294*, 359−369.

(31) Mukamel, S. *Principles of Nonlinear Optical Spectroscopy*; Oxford University Press: New York, 1995.

(32) Vos, M. H.; Jones, M. R.; Breton, J.; Lambry, J. C.; Martin, J. L. Vibrational Dephasing of Long- and Short-Lived Primary Donor Excited States in Mutant Reaction Centers of *Rhodobacter sphaeroides*. *Biochemistry* **1996**, *35*, 2687−92.

(33) Jordanides, X. J.; Scholes, G. D.; Shapley, W. A.; Reimers, J. R.; Fleming, G. R. Electronic Couplings and Energy Transfer Dynamics in the Oxidized Primary Electron Donor of the Bacterial Reaction Center. *J. Phys. Chem. B* **2004**, *108*, 1753−1765.

(34) Cheng, Y.-C.; Lee, H.; Fleming, G. R. Efficient Simulation of Three-Pulse Photon-Echo Signals with Application to the Determination of Electronic Coupling in a Bacterial Photosynthetic Reaction Center. *J. Phys. Chem. A* **2007**, *111*, 9499−9508.

(35) Zanni, M. T.; Ge, N. H.; Kim, Y. S.; Hochstrasser, R. M. Two-Dimensional IR Spectroscopy Can Be Designed to Eliminate the Diagonal Peaks and Expose Only the Crosspeaks Needed for Structure Determination. *Proc. Natl. Acad. Sci., U. S. A.* **2001**, *98*, 11265−11270.

(36) Smith, E. R.; Farrow, D. A; Jonas, D. M. Response Functions for Dimers and Square-Symmetric Molecules in Four-Wave-Mixing Experiments with Polarized Light. *J. Chem. Phys.* **2005**, *123*, 044102.

(37) Mančal, T.; Christensson, N.; Lukeš, V.; Milota, F.; Bixner, O.; Kauffmann, H. F.; Hauer, J. System-dependent Signatures of Electronic and Vibrational Coherences in Electronic Two-Dimensional Spectra. *J. Phys. Chem. Lett.* **2012**, *3*, 1497−1502.
(38) Cherepy, N. J.; Shreve, A. P.; Moore, L. J.; Boxer, S. G.; Mathies, R. A. Electronic and Nuclear Dynamics of the Accessory Bacteriochlorophylls in Bacterial Photosynthetic Reaction Centers from Resonance Raman Intensities. *J. Phys. Chem. B* **1997**, *101*, 3250−3260.
(39) Cherepy, N. J.; Shreve, a P.; Moore, L. J.; Boxer, S. G.; Mathies, R. A. Temperature Dependence of the Q_Y Resonance Raman Spectra of Bacteriochlorophylls, the Primary Electron Donor, and Bacteriopheophytins in the Bacterial Photosynthetic Reaction Center. *Biochemistry* **1997**, *36*, 8559−66.
(40) Zazubovich, V.; Tibe, I.; Small, G. J. Bacteriochlorophyll *a* Franck-Condon Factors for the $S_0 \rightarrow S_1(Q_y)$ Transition. *J. Phys. Chem. B* **2001**, *105*, 12410−12417.
(41) Womick, J. M.; Moran, A. M. Vibronic Enhancement of Exciton Sizes and Energy Transport in Photosynthetic Complexes. *J. Phys. Chem. B* **2011**, *115*, 1347−1356.
(42) Womick, J. M.; West, B. A.; Scherer, N. F.; Moran, A. M. Vibronic Effects in the Spectroscopy and Dynamics of C-Phycocyanin. *J. Phys. B, At. Mol. Opt. Phys.* **2012**, *45*, 154016.
(43) Reimers, J. R.; Hush, N. S. The Nature of the Near-Infrared Electronic Absorption at 1250 nm in the Spectra of the Radical Cations of the Special Pairs in the Photosynthetic Reaction Centers of *Rhodobacter sphaeroides* and *Rhodopseudomonas viridis*. *J. Am. Chem. Soc.* **1995**, *117*, 1302−1308.
(44) Read, E. L.; Engel, G. S.; Calhoun, T. R.; Mancal, T.; Ahn, T. K.; Blankenship, R. E.; Fleming, G. R. Multidimensional Ultrafast Spectroscopy Special Feature: Cross-Peak-Specific Two-Dimensional Electronic Spectroscopy. *Proc. Natl. Acad. Sci., U. S. A.* **2007**, *104*, 14203−14208.
(45) Schlau-Cohen, G. S.; Calhoun, T. R.; Ginsberg, N. S.; Read, E. L.; Ballottari, M.; Bassi, R.; van Grondelle, R.; Fleming, G. R. Pathways of Energy Flow in LHC II from Two-Dimensional Electronic Spectroscopy. *J. Phys. Chem. B* **2009**, *113*, 15352−15363.
(46) Butkus, V.; Zigmantas, D.; Abramavicius, D.; Valkunas, L. Distinctive Character of Electronic and Vibrational Coherences in Disordered Molecular Aggregates. *Chem. Phys. Lett.* **2013**, *587*, 93−98.